Structural and Rheological Properties of Hydrophobically Modified Polysaccharide Associative Networks

ARTICLE *in* LANGMUIR · APRIL 2004

Impact Factor: 4.46 · DOI: 10.1021/la036395s · Source: PubMed

4 AUTHORS, INCLUDING:

François Boué
French National Centre for Scientific Research
211 PUBLICATIONS **4,441** CITATIONS

SEE PROFILE

Eric Buhler
Paris Diderot University
61 PUBLICATIONS **1,346** CITATIONS

SEE PROFILE

Structural and Rheological Properties of Hydrophobically Modified Polysaccharide Associative Networks

Catherine Esquenet,[†] Pierre Terech,[‡] François Boué,[§] and Eric Buhler*[,†,||]

Centre de Recherches sur les Macromolécules Végétales (CERMAV), UPR-CNRS 5301, University Joseph Fourier, BP 53, 38041 Grenoble Cedex 9, France, Laboratoire Physico-Chimie Moléculaire, DRFMC/SI3M, CEA-Grenoble, 17, rue des Martyrs, 38054 Grenoble Cedex 9, France, Laboratoire Léon Brillouin (CEA-CNRS), CEA Saclay, 91191 Gif-sur-Yvette, France, and Groupe de Dynamique des Phases Condensées, UMR-CNRS 5581, cc26, University Montpellier 2, 34095 Montpellier Cedex 5, France

Received December 18, 2003. In Final Form: February 23, 2004

The phase behavior of hydrophobically modified chitosans (HMCs) in aqueous solution has been investigated using scattering and rheology experiments. We observed four regions on the phase diagram of the associative polymer: (i) a supernatant phase (unimers phase) at low polymer concentration; (ii) a dilute solution of intermolecularly bridged flowerlike micelles at intermediate concentration; (iii) an associative gel phase at high polymer content; and (iv) a phase separation. In the present paper, we discuss the structural and dynamical properties of the HMC associative networks ($c > c^*$) at a fixed hydrophobic degree of substitution of 2% and fixed alkyl side chains (stickers) length C8 (domains iii and iv of the phase diagram). As the polymer concentration is increasing, a connecting network is formed from the percolation of bridges between micellar aggregates. In this regime, small-angle neutron scattering and light scattering measurements show that ∼50-nm flower aggregates are acting like junction points in the network. The effect of the concentration, the stress, and the shear on the structure of the network is discussed. In particular, we observe bridge-to-loop transitions and then the formation of microgels or a low-connected network under shear. Therefore, our results are compared to recent theoretical models and to the results reported for telechelic systems.

1. Introduction

Over the past two decades, hydrophobically modified water-soluble polymers or so-called associating polymers have found an increasing number of applications. As a result of their remarkable thickening properties, they are used in paints, in cosmetics, for enhanced oil recovery, and so forth.[1−5] These new materials are water-soluble polymers bearing highly hydrophobic groups.[6−8] Also, some studies have been devoted to hydrophobically modified polyelectrolyte polysaccharides, that is, polysaccharides with low levels of hydrophobic groups (i.e., 1−5%).[9−12] Hydrophobically associating polyelectrolytes have shown unusual rheological features and high solubilization properties in aqueous media. These properties arise from the inter- or intramolecular interactions among hydrophobic groups, providing hydrophobic microdomains in an isotropic aqueous solution. In the present work, we have examined the structure and the dynamics of hydrophobically modified chitosans (HMCs) with a hydrophobic substitution degree of 2%. The HMC consists of alkyl side chains (hereafter called stickers) covalently linked to the polyelectrolyte chitosan backbone. In acid conditions, chitosan is water-soluble as a result of the presence of protonated amino groups, and it exhibits a polyelectrolyte character. The length and the number of alkyl side chains along the polycationic backbone control the degree of hydrophobicity of HMC.

In a previous study, we have examined the structure and the phase behavior of dilute aqueous HMC solutions in the presence of 0.3 M acetic acid and 0.05 M sodium acetate.[12] The aggregation process and the structure of the micelles in the dilute regime were discussed. Figure 1 shows the sequence of phase behaviors determined in the alkyl chitosan concentration−alkyl side chain length plane at fixed temperature $T = 25$ °C and at a fixed degree of substitution of 2% (by 2% we mean that 2% of the monomers carry a hydrophobic graft). The excess salt concentration being equal to 0.05 M, the charges of the polyelectrolyte main chain are screened. The partial phase diagram was obtained for the polymer concentration varying from 0 to 10^{-1} g/cm^3 and for an alkyl side chain

* To whom correspondence should be addressed: E. Buhler, Groupe de Dynamique des Phases Condensées (GDPC), UMR 5581, CC26, University of Montpellier 2, 34095 Montpellier Cedex 5, France. Phone: 33 (0)4 6714 3982. Fax: 33 (0)4 6714 4637. E-mail: buhler@gdpc.univ-montp2.fr.

[†] University Joseph Fourier.

[‡] CEA-Grenoble.

[§] CEA Saclay.

[||] University Montpellier 2.

(1) *Principles of Polymer Science and Technology in Cosmetics and Personal Care*; Goddard, E. D., Gruber, J. V., Eds.; Marcel Dekker: New York, 1999.

(2) McCormick, C. L.; Bock, J.; Schults, D. N. *Encyclopedia of Polymer Science and Engineering*; John Wiley: New York, 1989; Vol. 17, p 730.

(3) Bock, J.; Varadaraj, R.; Schultz, D. N.; Maurer, J. J. In *Macromolecular Complexes in Chemistry and Biology*; Dubin, P. L., Bock, J., Davies, R. M., Schultz, D. N., Thies, C., Eds.; Springer-Verlag: Berlin, 1994; p 33.

(4) *Polymers as Rheology Modifiers*; Schultz, D. N., Glass, J. E., Eds.; Advances in Chemistry Series 462; American Chemical Society: Washington, D.C., 1991.

(5) *Hydropilic Polymer, Performance with Environmental Acceptability*; Glass, J. E., Eds.; Advances in Chemistry Series 248; American Chemical Society: Washington, D.C., 1996.

(6) Petit, F.; Iliopoulos, I.; Audebert, R.; Szönyi, S. *Langmuir* **1997**, *13*, 4229.

(7) Tanaka, R.; Meadows, J.; Williams, P. A.; Phillips, G. O. *Macromolecules* **1992**, *25*, 1304.

(8) Biggs, S.; Hill, A.; Selb, J.; Candau, F. *J. Chem. Phys.* **1992**, *96*, 1505.

(9) Lee, K. Y.; Jo, W. H.; Kwon, I. C.; Kim, Y. H.; Jeong, S. Y. *Langmuir* **1998**, *14*, 2329.

(10) Kjøniksen, A. L.; Iversen, C.; Nyström, B.; Nakken, T.; Palmgren, O. *Macromolecules* **1998**, *31*, 8142.

(11) Kjøniksen, A. L.; Nyström, B.; Iversen, C.; Nakken, T.; Palmgren, O.; Tande, T. *Langmuir* **1997**, *13*, 4948.

(12) Esquenet, C.; Buhler, E. *Macromolecules* **2001**, *34*, 5287.

10.1021/la036395s CCC: $27.50
Published on Web 04/02/2004

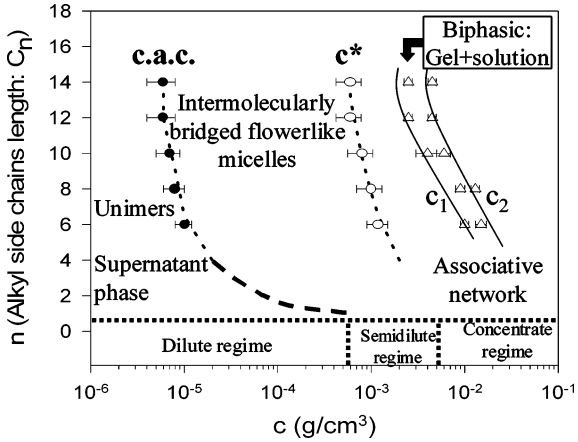

Figure 1. Sequence of phase behaviors of the HMC in the alkyl side chains length−polymer concentration plane at fixed temperature $T = 25$ °C and fixed degree of alkylation 2%. The points (●) represent the unimers−micelles transition (i.e., the cac deduced from SLS experiments, see Figure 3), the points (○) represent the micelles−network transition (i.e., the concentration c^* deduced from viscosity measurements, see Figure 2), and the points (△) represent the limits of the phase separation (i.e., the concentrations c_1 and c_2). C_n defines the length of the alkyl side chains, with n varying from 6 to 14. The phase behavior of the UMC (i.e., C0) is also represented.

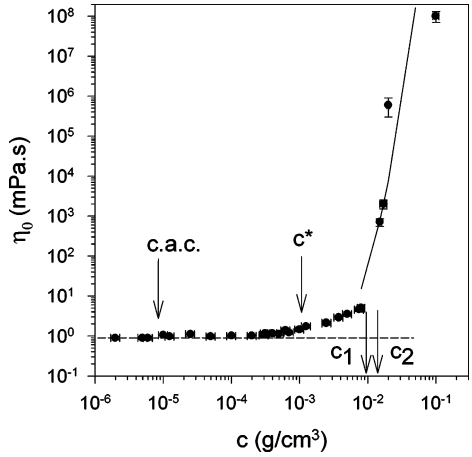

Figure 2. Variation of the zero-shear solution viscosity with the C8 HMC concentration. Arrows indicate the concentrations cac, c^*, c_1, and c_2. The black line represents the fit of the data obtained using eq 13 in the regime $c \gg c^*$.

length varying from C6 to C14 (i.e., the number of atoms of carbon in a sticker varies from 6 to 14). The phase behavior of the unmodified chitosan (UMC) characterized by an alkyl side chain length equal to zero, that is, C0, is also represented in Figure 1. The phase behavior of the UMC in solution shows the classical sequence[13] dilute regime, semidilute regime, and concentrate regime. Upon increasing polymer concentration, we have identified four regions on the partial phase diagram:

(i) At concentrations below the critical aggregation concentration ($c <$ cac) is a supernatant phase. This phase corresponds to free isolated HMC polymer chains dissolved in the solvent (hereafter called unimers, i.e., single macromolecules) characterized by a hydrodynamic radius equal to $R_{H,unimers} = 14$ nm (for our C8 HMC samples).

(ii) At intermediate polymer contents (cac $< c < c^*$) is a dilute solution of intermolecularly bridged "flowerlike" micelles (association of p unimers) that does not exhibit an increase of the solution viscosity. These micelles, characterized by a ratio $(R_H/R_G)_{micelles} \sim 1.65$, are not interconnected and are diluted in the solvent. In our previous work,[12] the light scattering study of the aggregation process of these micelles showed that the aggregation number, equal to $p = 15-20$ (i.e., 500 hydrophobic grafts in a micelle), and the size of the micelles, $R_{G,micelles} = 90$ nm, are constant over the whole regime cac $< c < c^*$, as predicted by the classical micellization theory.[14,15] Intrapolymer associations lead to the formation of "flowerlike" aggregates, with $m \gg 1$ stickers per hydrophobic core. The concurrent interpolymer associations link the flowerlike aggregates together, and, thus, dilute intermolecularly bridged flowerlike micelles are formed.[16−20] Also, unimers (isolated nonassociated chains) were found to coexist with the micelles, as expected.[12,14,15,21]

(iii) At higher polymer concentrations ($c > c^*$), the system exhibits a large increase of the solution viscosity and a gel-like behavior (associative network). Viscosity measurements indicated then the establishment of a network.

(iv) A phase separation between a solution and a gel-like phase is observed for concentrations ranging from c_1 to c_2 in the regime $c > c^*$.

The points corresponding to micelles−gel transitions ($c = c^*$) were deduced from the viscosity measurements. c^* corresponds to the concentration for which we observe a large increase of the solution viscosity, that is, the concentration at which we observe a departure from the dilute linear regime. Figure 2 shows the polymer concentration dependence of the solution viscosity for a HMC sample characterized by C8 alkyl side chains. The cac was determined by static light scattering (SLS) experiments. For concentrations below the cac, the measured molecular weight corresponds to the mass of a free chain ($M_{w,unimers} = 197\,600$ g/mol for the C8 sample). For concentrations larger than the cac, the molecular weight and then the intensity at zero-wave vector, $I(q^2 = 0)$, are increasing strongly with the polymer concentration and correspond to the growth process of associating polymer micelles. In Figure 3, $I(q^2 = 0)$ is plotted as a function of the polymer concentration for the HMC C8 sample.

The number m of stickers per hydrophobic microdomain depends on the length, on the chemical nature, and on the substitution degree of the stickers and may vary from 2 to 100.[22−27] In our case, the strong hydrophobic character of the alkyl side chains and the low degree of substitution equal to 2% imply three important consequences: (i) We

(13) Buhler, E.; Rinaudo, M. *Macromolecules* **2000**, *33*, 2098.
(14) Tuzar, Z.; Kratochvil, P. *Surf. Colloid Sci.* **1992**, *15*, 1.
(15) Halperin, A.; Tirrel, M.; Lodge, T. P. *Adv. Polym. Sci.* **1991**, 100.
(16) Yusa, S. I.; Hashidzume, A.; Morishima, Y. *Langmuir* **1999**, *15*, 8826.
(17) Dobrynin, A. V.; Rubinstein, M. *Macromolecules* **2000**, *33*, 8097.
(18) Halperin, A. *Macromolecules* **1991**, *24*, 1418.
(19) Semenov, A. N.; Joanny, J. F.; Khokhlov, A. R. *Macromolecules* **1995**, *28*, 1066.
(20) Yusa, S. I.; Kamachi, M.; Morishima, Y. *Langmuir* **1998**, *14*, 6059.
(21) Buhler, E.; Dobrynin, A. V.; DeSimone, J. M.; Rubinstein, M. *Macromolecules* **1998**, *31*, 7347.
(22) Regulado, E.; Selb, J.; Candau, F. *Macromolecules* **1999**, *32*, 8580.
(23) Williams, C. E. In *Multiphase Macromolecular Systems*; Culbertson, B. M., Ed.; Plenum Press: New York, 1989; Vol. 6.
(24) Moore, R. B.; Bittencourt, D.; Gauthier, M.; Williams, C. E.; Eisenberg, A. *Macromolecules* **1991**, *24*, 1376.
(25) Broze, G.; Jerome, R.; Teyssie, P. *Macromolecules* **1983**, *16*, 996.
(26) Balsara, N. P.; Tirrel, M.; Lodge, T. P. *Macromolecules* **1991**, *24*, 1975.
(27) Vasilevskaya, V. V.; Potemkin, I. I.; Khokhlov, A. R. *Langmuir* **1999**, *15*, 7918.

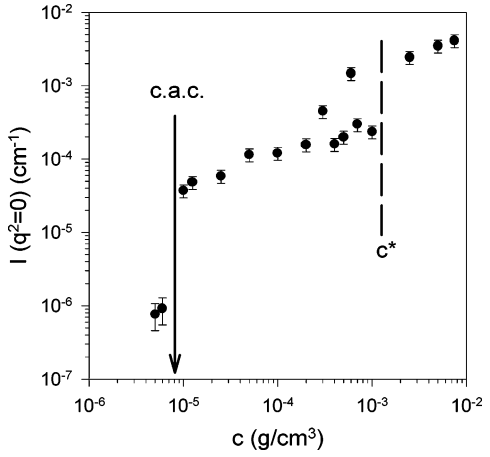

Figure 3. Light scattering intensity at zero angle as a function of the C8 HMC concentration. The arrow indicates the cac, and the vertical dashed line represents the transition between dilute micelles and the associative gel regime.

observe the formation of flowerlike micelles (intermolecularly bridged flowerlike micelles) in the dilute regime in which hydrophobic domains ($m \gg 1$) formed from alkyl associations are surrounded by loops of chitosan segments. The distance between two hydrophobic grafts, ~250 Å, allows the chain to easily form loops and then flowerlike structures. (ii) The grafts being sufficiently hydrophobic, combined static and dynamic light scattering (DLS) experiments[12] indicated that micelle formation follows a closed association mechanism (constant aggregation number p) and that the micelles conserve their size (~90 nm) and their number of alkyl side chains (~500) over the whole dilute concentration range cac $< c < c^*$. (iii) The aggregates will keep their flowerlike structure in the regime $c \gg c^*$. In this regime, an open secondary association process leading to the formation of bridges between neighboring micelles is occurring as the polymer concentration is increasing. In the regime $c > c^*$, the solution is completely filled with associated polymer structures. A connecting network is formed from the percolation of bridges leading to a large increase in the solution viscosity (see Figure 2). In this regime, flower aggregates are predicted to act as network junctions.[28] We will see in the results section that small-angle neutron scattering (SANS) and DLS experiments support such an explanation for the structure of the network.

Semenov and Rubinstein have described the structural and dynamical properties of associating polymers with many stickers ($f \gg 1$) per chain-forming networks of interconnected large flowerlike aggregates with many stickers per hydrophobic core ($m \gg 1$) in a recent theoretical study.[28] In particular, in the regime $c \gg c^*$ the number of bridges becomes larger than the number of loops at elevated polymer concentrations. The dynamics and the structure of telechelic polymer solutions with two end stickers per macromolecule ($f = 2$) and with large aggregates ($m \gg 1$) were already considered in many recent experimental and theoretical studies.[19,29−33] In this context, our results will be compared to that of telechelic systems.

In the present paper, we report the results of the light scattering, SANS, and rheology experiments performed on HMC associative networks at a fixed hydrophobic degree of substitution of 2% and fixed stickers' length C8 in the presence of 0.3 M acetic acid and 0.05 M sodium acetate. In section 2 of the paper, we describe materials and experimental techniques used in this study. In section 3, we report the results of the experiments. The structural and rheological properties of the gel-like phase (domains iii and iv of the phase diagram) are also discussed in section 3.

2. Materials and Methods

2.1. Sample Characteristics. We have investigated solutions of the hydrophobically modified polysaccharide chitosans (HMC). Alkyl side chains are grafted to the main chitosan chain, which is a semirigid polyelectrolyte (the intrinsic persistence length of chitosan is roughly equal to 75 Å).[34] Chitosan is a polysaccharide from PROTAN composed of β 1→ 4 D-glucosamine units with a degree of *N*-acetylation equal to 12%. The polysaccharide chitosan belongs to a family of linear cationic biopolymers obtained from alkaline *N*-deacetylation of chitin, which is the second most abundant polymer in nature. The mass $M_w = 195\,000 \pm 5000$ g/mol and the polydispersity $M_w/M_n = 1.3$ of the UMC were determined by GPC and light scattering,[13,34] where M_w is the weight-average molecular weight and M_n is the number-average molecular weight. The contour length is equal to $L_c = 6000$ Å. The solutions were investigated in the polymer concentration range from 2×10^{-6} to 10^{-1} g/cm^3 at 25 °C and in the solvent 0.3 M acetic acid (CH_3COOH) in the presence of sodium acetate (CH_3COONa). The concentration of sodium acetate (excess of salt) was equal to 0.05 M. For a 0.3 M concentration in acetic acid, all the amino groups are protonated and chitosan exhibits a polyelectrolyte character.[13,34] This medium is a good solvent for the chitosan main chain[13,34] and a bad solvent for the alkyl side chains.

The hydrophobically modified samples were prepared by reaction with the amino groups of the backbone of the polymer chain with C6 to C14 aldehyde. The modification procedure employed here is similar to the method described earlier.[35,36] The degree of alkylation used in this work is equal to 2% and has been checked by ^{1}H NMR measurements[35] (2% of the monomers are bearing an alkyl chain). The HMCs are equivalent to their unmodified analogue; the main chitosan chain is the same for all samples investigated. The mass of the HMC sample was then calculated (for example, the mass of the C8 HMC is estimated to be equal to $M_w = 197\,600 \pm 5000$ g/mol). The length of the alkyl side chains was varied from C6 to C14.

2.2. Rheological Measurements. The rheological measurements were carried out with a Haake RS 100 stress rheometer using a cone−plate geometry (20- or 35-mm plate diameter and 2° cone angle). In oscillatory experiments, the explored frequency range was $0.001 \le f \le 100$ Hz.

The viscosity measurements were carried out using a Low-Shear 40 coaxial viscometer, within the range of polymer concentration from 2×10^{-6} to 8×10^{-3} g/cm^3. For elevated polymer contents, that is, for $8 \times 10^{-3} < c < 10^{-1}$ g/cm^3, the viscosity measurements (see Figure 4) were performed using the rheometer and a cone−plate geometry. The variation of the zero-shear viscosity η_0 with polymer concentration is presented in Figure 2.

2.3. Fluorescence Spectroscopy Measurements. Fluorescence spectroscopy studies were conducted using a Polarimeter 341 Perkin-Elmer spectrometer. Pyrene (at concentration of 4.9×10^{-7} mol/L, Aldrich 99%) was employed as a hydrophobic probe. Variations in the polarity of the probe's microenvironment are manifested as changes in the ratio of the intensity of the highest energy vibronic band in the emission spectrum (I_1 at 373 nm) to that of the band of third highest energy (I_3 at 384 nm). A variation

(28) Semenov, A. N.; Rubinstein, M. *Macromolecules* **2002**, *35*, 4821.
(29) Tam, K. C.; Jenkins, R. D.; Winnik, M. A.; Bassett, D. R. *Macromolecules* **1998**, *31*, 4149.
(30) Le Meins, J. F.; Tassin, J. F. *Macromolecules* **2001**, *34*, 2641.
(31) Raspaud, E.; Lairez, D.; Adam, M.; Carton, J. P. *Macromolecules* **1996**, *29*, 1269.
(32) Raspaud, E.; Lairez, D.; Adam, M.; Carton, J. P. *Macromolecules* **1994**, *27*, 2956.
(33) Lairez, D.; Adam, M.; Carton, J. P.; Raspaud, E. *Macromolecules* **1997**, *30*, 6798.
(34) Buhler, E.; Guetta, O.; Rinaudo, M. *Int. J. Polym. Anal. Charact.* **2000**, *6*, 155.
(35) Desbrières, J.; Rinaudo, M.; Chtcheglova, L. *Macromol. Symp.* **1997**, *113*, 135.
(36) Yalpani, M.; Hall, L. D. *Macromolecules* **1984**, *17*, 272.

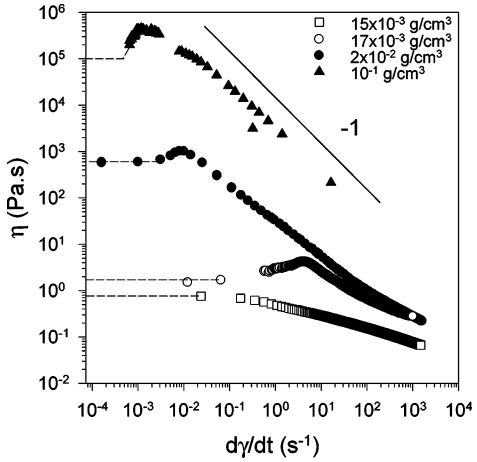

Figure 4. Dependence of the viscosity on the shear rate for $c = 15 \times 10^{-3}$ g/cm^3 (□), $c = 17 \times 10^{-3}$ g/cm^3 (○), $c = 20 \times 10^{-3}$ g/cm^3 (●), and $c = 10^{-1}$ g/cm^3 (▲). The dashed lines represent the Newtonian plateaus. The zero-shear viscosity is obtained with a relatively large error bar.

in the I_1/I_3 ratio provides information on the presence and structure of hydrophobic domains in a system.

2.4. SLS. SLS and DLS experiments were performed by means of a spectrometer equipped with an argon ion laser (Spectra Physics model 2020) operating at $\lambda = 488$ nm, an ALV-5000 correlator (ALV, Langen-Germany Instruments), a computer-controlled and stepping-motor-driven variable angle detection system, and a temperature-controlled sample cell. The temperature was 25 ± 0.1 °C unless otherwise noted. The scattering spectrum was measured through a band-pass filter (488 nm) and a pinhole (200 μm for the static experiments and 100 μm or 50 μm for the dynamic experiments) with a photomultiplier tube (ALV).

In the SLS experiments, the excess of the scattered intensity $I(q)$ was measured with respect to the solvent, where the magnitude of the scattering wave vector q is given by

$$q = \frac{4\pi n}{\lambda} \sin\frac{\theta}{2} \tag{1}$$

In eq 1, n is the refractive index of the solvent (1.34 for the water at 25 °C), λ is the wavelength of light in the vacuum, and θ is the scattering angle. In our experiments, the scattering angle θ was varied between 20 and 150°, which corresponds to scattering wave vectors q in the range from 6×10^{-4} to 3.2×10^{-3} Å^{-1}. The absolute scattering intensities $I(q)$ (cm^{-1}; i.e., the excess Rayleigh ratio) were deduced by using a toluene sample reference for which the excess Rayleigh ratio is well-known, that is, 40×10^{-6} cm^{-1} at 488 nm.[37]

A virial expression for the osmotic pressure can be used in the dilute regime to deduce the following relationship:

$$\frac{Kc}{I(q, c)} = \frac{1}{M_w}\left[1 + q^2\frac{R_G^2}{3} + ...\right] + 2A_2Q(q, c)c + ... \tag{2}$$

The function $Q(q, c)$ is approximately unity for flexible polymer chains but not for spheres,[37] $Q(0, c)$ is equal to 1 in any case, c is the polymer concentration, and A_2 is the second virial coefficient, which describes the polymer−solvent interactions. The scattering constant is $K = 4\pi^2n^2(dn/dc)^2/N_A\lambda^4$, where dn/dc is the refractive index increment and N_A is Avogadro's number. The dn/dc of the polysaccharide chitosan in the solvent composed of 0.3 M acetic acid + sodium acetate is equal to 0.195 cm^3/g.[13,34] The plots of $c/I(q, c)$ versus q^2 were extrapolated to $q = 0$ to give intercepts $c/I(0, c)$. If the length scale q^{-1} is sufficiently large compared to the radius of gyration R_G of the polymers, the form factor obeys Guinier's law and the apparent radius of gyration $R_{G,app}$ can be determined from the intercept and the initial slope of these plots using a scattering inverse Lorentzian law of the form[37]

$$\frac{c}{I(q, c)} = \frac{c}{I(0, c)}\left[1 + \frac{q^2R_{G,app}^2}{3}\right] \quad \text{if} \quad qR_G \ll 1 \tag{3}$$

The weight average molecular weight[37] M_w can be obtained from

$$\frac{I(0, c)}{Kc} = M_{w,app} = M_w(1 - 2A_2M_wc) \tag{4}$$

The apparent mass $M_{w,app}$ of polymers in solution at a concentration c is given by extrapolation of the scattered intensity $I(q)/c$ to $q = 0$, while the apparent radius of gyration is obtained by a mean-square linear fit of the inverse of the scattered intensity versus q^2.

2.5. DLS. In the DLS experiments, the normalized time autocorrelation function $g^{(2)}(q, t)$ of the scattered intensity is measured.[37]

$$g^{(2)}(q, t) = \frac{\langle I(q, 0)\, I(q, t)\rangle}{\langle I(q, 0)\rangle^2} \tag{5}$$

The latter can be expressed in terms of the field autocorrelation function or equivalently in terms of the autocorrelation function of the concentration fluctuations $g^{(1)}(q, t)$ through

$$g^{(2)}(q, t) = A + \beta|g^{(1)}(q, t)|^2 \tag{6}$$

where A is the baseline and β is the coherence factor which in our experiments is equal to 0.7−0.9. The normalized dynamical correlation function $g^{(1)}(q, t)$ of polymer concentration fluctuations is defined as

$$g^{(1)}(q, t) = \frac{\langle \delta c(q, 0)\, \delta c(q, t)\rangle}{\langle \delta c(q, 0)^2\rangle} \tag{7}$$

where $\delta c(q, t)$ and $\delta c(q, 0)$ represent fluctuations of the polymer concentration at time t and 0, respectively.

In our experiments, the inspection of the angular dependence shows that some relaxations are diffusive with the characteristic time τ inversely proportioned to q^2. The extrapolation of $(\tau q^2)^{-1}$ to $q = 0$ yields the value of the mutual diffusion constant D. The latter is related to the average hydrodynamic radius R_H of the objects through[37]

$$D = \frac{kT}{6\pi\eta_sR_H} = \left(\frac{1}{\tau q^2}\right)_{q^2=0} \tag{8}$$

where k is the Boltzman constant, η_s is the solvent viscosity, and T is the absolute temperature.

To determine the average relaxation time τ, we used the Contin method based on the inverse Laplace transform of $g^{(1)}(q, t)$.[38] If the spectral profile of the scattered light can be described by a multi-Lorentzian curve, then $g^{(1)}(q, t)$ can be written as

$$g^{(1)}(q, t) = \int_0^\infty G(\Gamma)\exp(-\Gamma t)\, d\Gamma \tag{9}$$

where $G(\Gamma)$ is the normalized decay constant distribution. This method is more appropriate for the solutions characterized by several relaxation mechanisms.

The studied solutions and gels being very viscous in the regime $c \gg c^*$, the samples cannot be filtered directly into the light scattering cells. To eliminate the dusts, we proceeded as follows: an initial 5×10^{-3} g/cm^3 alkyl chitosan solution was prepared in the solvent 0.3 M CH_3COOH/0.05 M CH_3COONa. Prior to preparation, the solvent was filtered two times through a 0.1-μm Sartorius cellulose nitrate membrane. After 3 days of mixing at $T = 4$ °C, the initial homogeneous solution was slowly filtered successively through an 8-μm, through a 3-μm, and then through a 1.2-μm nitrate cellulose membrane. Very small amounts of

(37) *An Introduction to Dynamic Light Scattering by Macromolecules*; Schmitz, K. S., Ed.; Academic Press, Inc.: San Diego, 1990.

(38) Provencher, S. W. *Makromol. Chem.* **1985**, *82*, 632.

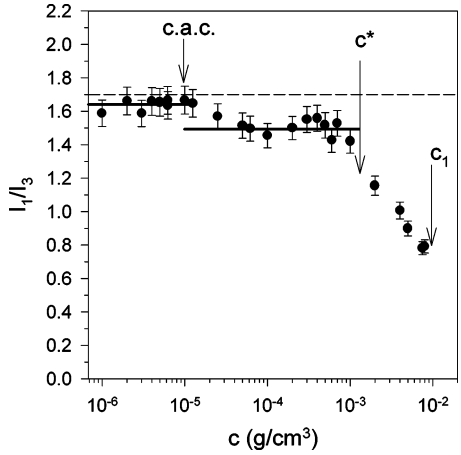

Figure 5. Variation of the characteristic ratio I_1/I_3 as a function of the C8 HMC concentration obtained using fluorescence experiments employing pyrene as a hydrophobic probe. The dashed line represents the value of the solvent ~1.7.

alkyl chitosan derivative may be lost in the filters. To concentrate these dust-free initial 5×10^{-3} g/cm^3 solutions, we used a Rotavapor. Varying the amount of evaporated solvent, solutions of the desired concentrations were, thus, dust-free prepared. The absence of any significant aging effects was noticed with the prepared specimens.

2.6. SANS. SANS experiments were carried out on the spectrometer PACE in Léon Brillouin Laboratory at Saclay (Orphée reactor, France). The chosen incident wavelength λ depends on the set of experiments, as follows. For a given wavelength, the range of the amplitude of the transfer wave vector q was selected by changing the detector distance D. Three sets of sample-to-detector distances and wavelengths were chosen ($D = 4.6$ m, $\lambda = 13 \pm 1.00$ Å; $D = 3.06$ m, $\lambda = 10 \pm 0.50$ Å; and $D = 1.1$ m, $\lambda = 5 \pm 0.50$ Å) so that the following q ranges were respectively available: $3.15 \times 10^{-3} \le q$ (Å^{-1}) $\le 3.36 \times 10^{-2}$, $6.1 \times 10^{-3} \le q$ (Å^{-1}) $\le 6.48 \times 10^{-2}$, and $3.43 \times 10^{-2} \le q$ (Å^{-1}) $\le 3.55 \times 10^{-1}$. Measured intensities were calibrated to absolute values (cm^{-1}) using the normalization by the attenuated direct beam classical method. Standard procedures to correct the data for the transmission, detector efficiency, and backgrounds (solvent, empty cell, electronic, and neutronic background) were done.

It is possible to combine data from light and neutron static scattering covering these different but overlapping q ranges. Both the neutron and the light scattering data have been normalized to give absolute scale units in cm^{-1}. Therefore, it is still necessary to rescale the SLS data to give the overlap with the SANS data. This scaling factor is equal to the ratio between the SANS contrast and the SLS contrast. The light scattering intensity at each q value was adjusted by this constant factor so that the SLS data overlap with the SANS data in the region of comparable q. The scattering profiles cover then a q range of nearly 3 decades.

3. Results and Discussion

3.1. Fluorescence Spectroscopy. The existence of the different regimes in solutions of associative polysaccharides bearing multiple hydrophobic groups described in Figure 1 (phase diagram) is supported from fluorescence spectroscopy employing pyrene as a hydrophobic probe. The variation in the characteristic ratio I_1/I_3 as a function of the C8 alkyl chitosan concentration is depicted in Figure 5. In this Figure, we observe a value for the characteristic ratio below the value measured and that expected for pyrene in an aqueous environment (for the solvent $I_1/I_3 \sim 1.7$) over the whole investigated concentration range. In a first regime, which corresponds to the dilute unimers phase ($c <$ cac), the value of I_1/I_3 is slightly smaller than 1.7 and corresponds to the intrapolymer hydrophobic associations which may lead to the formation of a polymer micelle made up with a single C8 HMC macromolecular chain ("unimolecular micelle" or "unimermicelle" of size

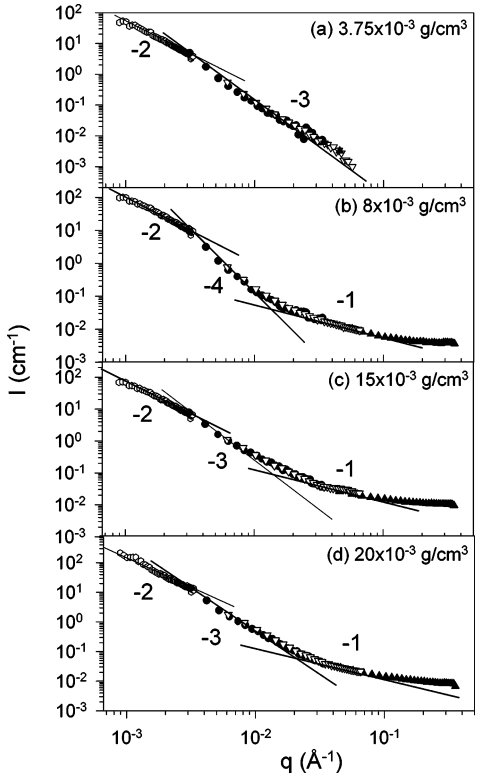

Figure 6. log−log variation of the scattered intensity with q over the four investigated q ranges [SLS (○) and SANS (●, ▽, and ▲)] for four C8 HMC concentrations in the regime $c > c^*$: (a) $c = 3.75 \times 10^{-3}$ g/cm^3, (b) $c = 8 \times 10^{-3}$ g/cm^3 (below the phase separation), (c) $c = 15 \times 10^{-3}$ g/cm^3 (above the phase separation), and (d) $c = 20 \times 10^{-3}$ g/cm^3.

$R_{H,unimers} = 14$ nm).[12,39] The second regime appears for concentrations larger than the cac, cac $= (8 \pm 2) \times 10^{-6}$ g/cm^3, the latter being determined from SLS experiments (see Figure 3). The data reveal a relatively constant I_1/I_3 (~1.5) across this regime cac $< c < c^*$ and correspond to the formation of micelles characterized by a constant number of hydrophobic grafts.[12] Finally, at polymer concentrations exceeding $c^* \sim 10^{-3}$ g/cm^3, at which viscosity experiments indicated the establishment of a network, the characteristic ratio is strongly and continuously decreasing. Therefore, the number m of hydrophobic stickers in flower aggregates is increasing with polymer concentration. In this regime ($c > c^*$), one expects the formation of bridges between neighboring flower aggregates and then the formation of an associative network.[28−30,40] Flower aggregates with $m \gg 1$ are acting like junction points in the network.[28] SANS, DLS, and rheology experiments support the hypothesis.

3.2. SLS and SANS. Scattering experiments were carried out in the associative gel phase ($c > c^*$) above and below the phase separation (i.e., above and below the biphasic domain). The results obtained using combined SLS and SANS measurements are presented in Figure 6 for four different polymer concentrations. In this figure representing the variation of the scattered intensity with q (log−log plot) over the four investigated q ranges (SLS and SANS), it is difficult to say whether there is a Guinier regime or not in the low-q SLS domain. In the low-q-range domain, the scattering profile evolves from a Gaussian decay [where the intensity $I(q)$ is proportional to q^{-2}, SLS domain] to a q^{-3} decrease. The latter corre-

(39) Yamamoto, H.; Morishima, Y. *Macromolecules* **1999**, *32*, 7469.
(40) Noda, T.; Hashidzume, A.; Morishima, Y. *Langmuir* **2001**, *17*, 5984.

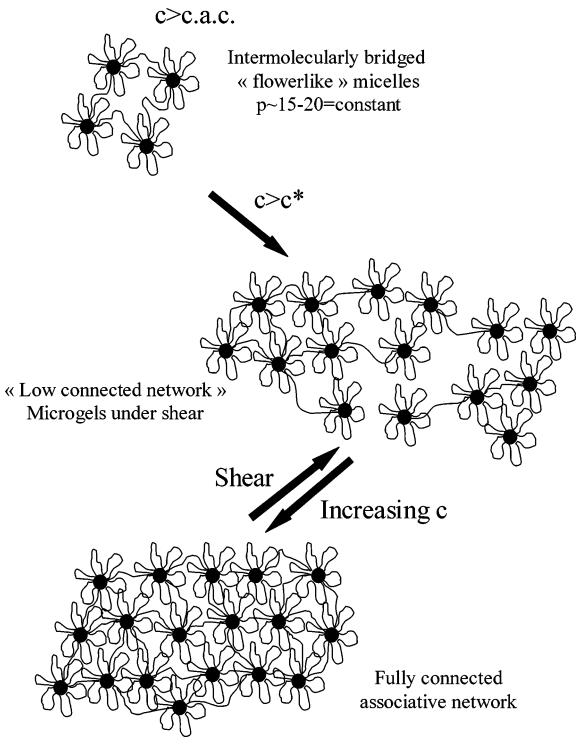

Figure 7. Schematic diagram depicting the effect of the concentration and of the shear on the structure of the associative network.

sponds to the signal of aggregates. We observe a q^{-4} dependence for the concentration 8×10^{-3} g/cm^3, that is, just before the phase separation, a small domain where aggregates are certainly more dense and more compact (see section 3.5). The SANS experiments show clearly the presence of aggregates. The characteristic objects that adopt a Gaussian distribution are certainly the chitosan coils constituting the associative network. The q^{-3} (or q^{-4}) regime corresponds then to the signal of the flower aggregates. A picture of these kind of networks is represented in Figure 7 and corresponds to the model described by Semenov and Rubinstein.[28] In the high-q SANS regime, the variation of the scattered intensity with q shows a transition from a q^{-1} to a q^{-3} dependence (when q decreases), the latter being characteristic of the flower aggregates. The q^{-1} dependence corresponds to the characteristic rod behavior of the semirigid chitosan chains when we look at smaller distances than the persistence length[34] $L_p \sim 75$ Å and where the form factor of a wormlike chain varies as q^{-1}. The scattering due to the presence of the aggregates overlaps the rod-to-coil transition of the chitosan chains (transition from a q^{-1} to a q^{-2} dependence when q decreases) usually observed in classical wormlike chains solutions.[41,42] The crossover q value at which we observe a transition between the q^{-1} and the q^{-3} regime gives certainly a lower bound for L_p.[41,42] Finally, in the high-q-range domain ($q > 0.1$ Å^{-1}), we observe a departure from the q^{-1}-rod behavior. But one must note that the scattering length scale q^{-1} is the same order in this regime as the length of a monomer unit (5 Å). We see then details of the monomer shape inside the solvent, which are beyond our scope.[37]

3.3. DLS. *3.3.1. Time Autocorrelation Function.* Parts a and b of Figure 8 show a typical autocorrelation function $g^{(1)}(q, t)$ obtained for HMC solutions for scattering angles

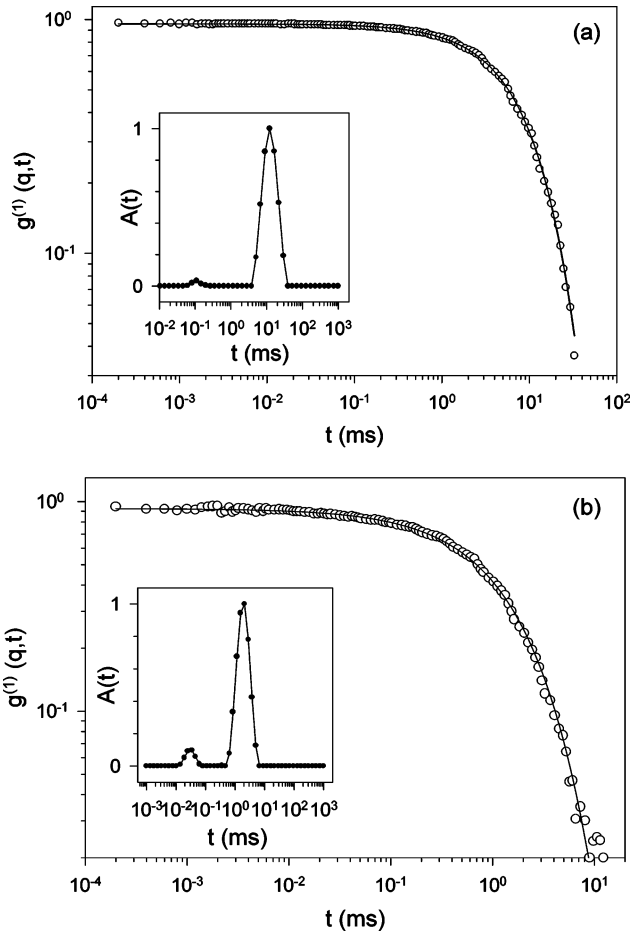

Figure 8. (a) Typical log−log representation of $g^{(1)}(q, t)$ for $\theta = 50°$ relative to a C8 HMC semidilute solution ($c > c^*$) at polymer concentration $c = 15 \times 10^{-3}$ g/cm^3. The slow relaxation time presents a q^{-2} dependence, and $\gamma = 1$. (b) A typical log−log representation of $g^{(1)}(q, t)$ for $\theta = 120°$ relative to a semidilute solution at $c = 15 \times 10^{-3}$ g/cm^3. In this case, τ_{slow} is q^{-3}-dependent and $\gamma = 2/3$. The black lines represent the fit of $g^{(1)}(q, t)$ obtained using eq 10. The results obtained using the classical Contin method are presented in the insets.

θ equal to 50 and 120°, respectively. The inset shows the normalized time distribution function $A(t)$ obtained using the classical Contin method. The DLS results obtained in the regime $c > c^*$ suggest two well-defined characteristic times for the relaxation function $g^{(1)}(q, t)$. The slow mode of the correlation function is characterized by a simple exponential function for low scattering angles (Figure 8a), while it is characterized by a stretched exponential function for large scattering angles (Figure 8b). This uncommon behavior is observed in whole the regime $c > c^*$ above and below the phase separation. To analyze the quasi-elastic light scattering data within this context, the scattered electric field time autocorrelation function $g^{(1)}(q, t)$ was fitted using the following general form:

$$g^{(1)}(q, t) = A_{fast}(q)e^{-(t/\tau_{fast})} + A_{slow}(q)e^{-(t/\tau_{slow})^{\gamma}} \quad (10)$$

with $A_{fast}(q) + A_{slow}(q) = 1$. $\tau_{fast}(q)$ and $\tau_{slow}(q)$ are respectively the fast and the slow characteristic relaxation time. $A_{fast}(q)$ and $A_{slow}(q)$ are the corresponding amplitudes. The results of the fit obtained using eq 10 show that $\gamma = 1$ (Figure 8a) for the low scattering angles and $\gamma \approx 2/3$ (Figure 8b) for the large scattering angles. The Contin method was used as a diagnostic tool to indicate the number of relaxation modes and to determine A_{fast} and τ_{fast}, the fast mode being characterized by relatively small

(41) Buhler, E.; Boué, F. *Eur. Phys. J. E* **2003**, *10*, 89.
(42) Buhler, E.; Boué, F. *Macromolecules* **2004**, *37*, 1600.

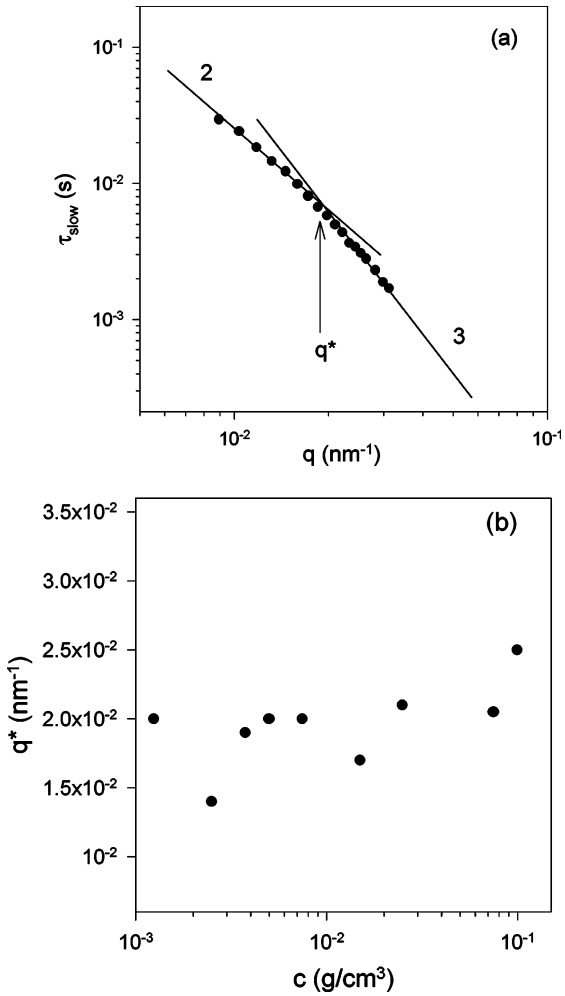

Figure 9. (a) Variation of the slow characteristic relaxation time with q measured in a $c = 15 \times 10^{-3}$ g/cm^3 solution ($c > c^*$). The transition between the regime where $\tau_{slow} \sim q^{-2}$ and the regime where $\tau_{slow} \sim q^{-3}$ is marked with q^*. (b) Variation of q^* with the polymer concentration c in the regime $c > c^*$; the experimental error is equal to 10%.

amplitudes. However, one should note that a very good agreement is found between the results obtained using the Contin method and eq 10.

3.3.2. Slow Relaxation Process. The inspection of Figure 9a, representing a typical variation of τ_{slow} with q for HMC solutions in the regime $c > c^*$, shows clearly that slow relaxation times are characterized by a q^{-2} dependence at low scattering angles ($\gamma = 1$) and by a q^{-3} dependence at large scattering angles ($\gamma \approx 2/3$). The transition between the characteristic regime where $\tau_{slow} \sim q^{-2}$ and $\gamma = 1$ and the characteristic regime where $\tau_{slow} \sim q^{-3}$ and $\gamma = 2/3$ is marked with q^* in Figure 9. In fact, the physical origin of the slow mode depends on the scattering wave vector. The $\tau_{slow} \sim q^{-2}$ dependence indicates that the slow mode is diffusive at low scattering wave vectors. Thus, it is possible to calculate a slow diffusion coefficient $D_{slow} = (1/\tau_{slow}q^2)_{q^2=0}$ in the low scattering angles domain. In the large scattering wave vectors domain, the q^{-3} dependence is consistent with internal modes dynamics.[32,43−46] The slowly fluctuating intensity could originate from objects (as long as the latter are not compact) whose characteristic length would be larger than the q^{-1} value explored in the light scattering experiments in the regime $q > q^*$. One can show that, in the case of linear polymers, the q^{-3} dependence of characteristic times corresponding to internal modes comes with a stretched exponential relaxation function having an exponent $\gamma = 2/3$. At large scattering angles, the experimental values of γ are close to that value in the whole investigated concentration range.

In our system, we observe the formation of a homogeneous associative network where flower aggregates are interconnected and are acting like junction points, the presence of the latter being clearly observed in our SANS measurements. The $\tau_{slow} \sim q^{-2}$ dependence observed for the low scattering angles should correspond to the diffusion of these flower aggregates. When we look at smaller distances, the scattering length scale q^{-1} is smaller than the size of the aggregates and we observed internal modes dynamics. The inverse of q^* should then correspond to the size (or the radius of gyration) of the aggregates. The inspection of Figure 9b, representing the variation of q^* with the polymer concentration, shows that the characteristic size of these aggregates is constant and equal to $q^{*-1} = 53 \pm 15$ nm over the whole regime $c > c^*$. Moreover, values of the hydrodynamic radius associated with the slow mode and calculated using D_{slow} and the zero-shear solution viscosity η_0 in the low angles domain are also constant and equal to $R_{H,slow} = kT/6\pi\eta_0 D_{slow}(q^2 = 0) = 58 \pm 15$ nm over the whole investigated concentration range. This excellent agreement between q^{*-1} and $R_{H,slow}$ supports the previous interpretation, which assigned the slow mode to the dynamics of aggregates. The radius of gyration of an "intermolecularly bridged flowerlike" micelle in the dilute regime being equal to 90 nm,[12] a value of 50 nm for the size of a flower aggregate is definitively reasonable. In the regime $c > c^*$, the increase of the number of bridges between neighboring flower aggregates with the polymer content does not influence the size of these aggregates. However, the increase of the density of these characteristic objects with the concentration is responsible for the increase of the scattered intensity at $q = 0$ in the regime $c > c^*$ observed in Figure 3.

3.3.3. Fast Relaxation Mode. The analysis of the fast mode shows clearly that the latter is diffusive with characteristic time τ_{fast} inversely proportional to q^2. Thus, it is possible to calculate a fast diffusion coefficient, $D_{fast} = (1/\tau_{fast}q^2)_{q^2=0}$, for each polymer concentration in the regime $c > c^*$ (see Figure 10a). For the origin of the fast mode, several assumptions can be made: (i) We can calculate a hydrodynamic size using the Stokes−Einstein relation (eq 8) and the value of D_{fast}. This hydrodynamic size, equal to ∼7 nm, can be attributed to the mesh size of the network. However, it is surprising to observe no decrease of the mesh size when the polymer concentration is increasing. (ii) This size could also be attributed to the hydrophobic cores of the aggregates. (iii) The last possibility is to attribute the fast mode to the free sticker diffusion process (sticker not associated in a hydrophobic core). The bond lifetime, τ_b, is given by the following expression:[28]

$$\tau_b = \tau_0 \exp \epsilon \qquad (11)$$

where $\tau_0 \sim \eta_s b^3/kT$ is the microscopic time characterizing sticker diffusion, that is, the time for a free graft to diffuse between two aggregates. This free sticker diffusion process is very fast and should correspond to the nondependent concentration fast diffusion coefficient measured in our DLS experiments. ϵkT is the activation energy for a sticker dissociation, and b is the length of a hydrophobic graft.

(43) Adam, M.; Delsanti, M. *J. Phys. Lett.* **1997**, *38*, L-271.
(44) Dubois-Violette, E.; de Gennes, P. G. *Physics* **1967**, *3*, 181.
(45) Akcasu, A. Z.; Benmouna, M.; Han, C. C. *Polymer* **1980**, *21*, 866.
(46) Esquenet, C.; Buhler, E. *Macromolecules* **2002**, *35*, 3708.

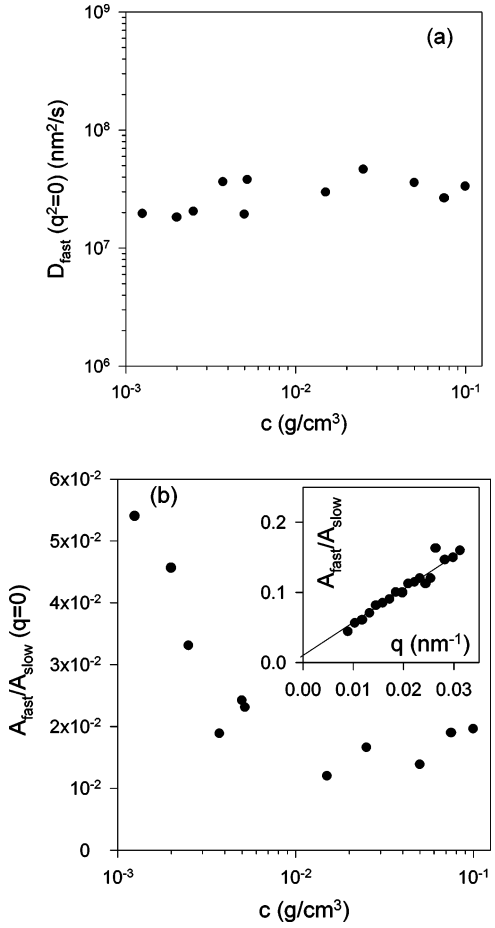

Figure 10. (a) Dependence of the fast diffusion coefficient on the polymer concentration in the regime $c > c^*$. (b) Concentration dependence of A_{fast}/A_{slow} ($q = 0$) in the regime $c > c^*$. The inset represents the variation of A_{fast}/A_{slow} with q for a $c = 15 \times 10^{-3}$ g/cm^3 solution. The experimental error is equal to 10%.

The decrease of the ratio A_{fast}/A_{slow} with polymer concentration and with the decrease of q can be observed in Figure 10b. These characteristic variations confirm that the slow mode is due to the signal of large aggregates.

3.4. Rheological Behavior. *3.4.1. Effect of the HMC Concentration.* Above the overlap concentration c^*, the solution is completely filled with associated flowerlike polymer structures. As the polymer concentration is increasing, an association process leading to the formation of bridges between neighboring flower aggregates is occurring.[28−33,40] A connecting network is then formed from the percolation of bridges leading to a large increase in the solution viscosity (see Figure 2). In this regime, polymer chains form a network structure where the flower aggregates act as network junctions[28−33,40] and are responsible for the $I \sim q^{-3}$ SANS signal and of the slow mode measured in DLS. We also observe the appearance of an elastic shear modulus for $c > c^*$. Our objective in the following part is to describe phenomenologically the rheological behavior at three different concentration regimes.

The variation of the storage modulus G' in C8 HMC solutions as a function of the stress amplitude σ at a fixed frequency $f = 1$ Hz is depicted in Figure 11 for three concentrations larger than c_2, that is, for concentrations above the phase separation. These experiments show that the networks' structure and behavior are very sensitive to the polymer concentration. At low polymer concentration ($c = 15 \times 10^{-3}$ g/cm^3, Figure 11a), we first observe an instantaneous and dramatic decrease (over 4 decades) of

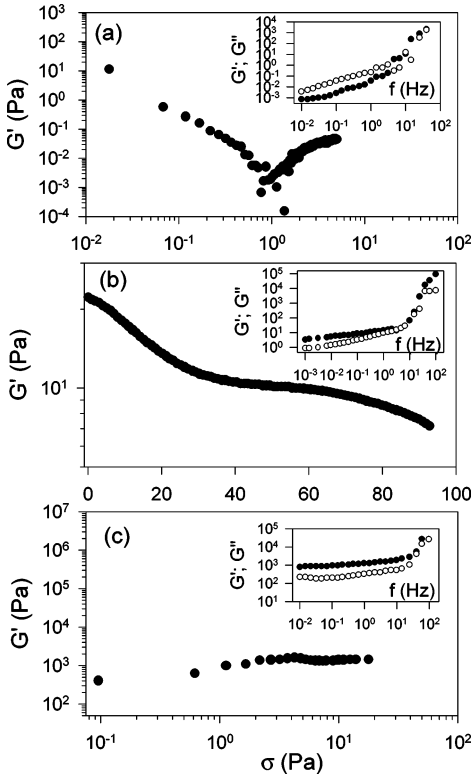

Figure 11. Variation of the storage modulus G' with the stress for (a) $c = 15 \times 10^{-3}$ g/cm^3, (b) $c = 20 \times 10^{-3}$ g/cm^3, and (c) $c = 10^{-1}$ g/cm^3. The insets represent storage (●) and loss (○) moduli as a function of frequency.

the elastic modulus G' under stress. This decrease is ascribed to the change in the connectivity of the associative network. Under stress, interpolymer associations responsible of the formation of bridges between the flower aggregates are easily broken, probably because the latter are not sufficiently numerous. At this concentration, we observe then a low-connected very weak network, with formation of a solution of nonconnected microgels under stress characterized by a very low G' value around 10^{-4} Pa. We observe a yield stress value around 1 Pa, which is a very weak value. The yield stress corresponds to the stress at which the system behaves like a liquid. Beyond the yield stress value σ^*, a subsequent increase of the elasticity may be due to a collapsing arrangement of the structure through the stickers. At this concentration, small deformation linear viscoelastic theory cannot apply; however, our description is purely phenomenological. At $c = 2 \times 10^{-2}$ g/cm^3 (see Figure 11b), the strength and cohesion of the network are significantly improved because the elastic shear modulus remains at larger values (around 10−15 Pa) within a broad range of applied stresses (0−90 Pa). Still, the elasticity is moderate and a remarkable intermediate plateau (in the 30−60 Pa range) is observed after a shear-thinned restructuring of the system. The absence of a linear domain at the beginning of the stress application could imply an inelastic distortion of the system. The associated yield value for such a system appears to be beyond the investigated stress range (not shown). At elevated stress, G' is decreasing as expected. This decrease is attributed to bridge-to-loop transitions and is leading to the formation of a liquidlike solution. With further increase in polymer content, we obtain a fully connected associative network, that is, a gel with a solidlike rheological behavior (see Figure 11c). In this concentration regime ($c = 10^{-1}$ g/cm^3), the network is very rigid and corresponding values of the elastic shear modulus

are almost constant in the stress range and 2 orders of magnitude higher (~1000 Pa). The flat variation observed for G' as a function of the frequency (see inset) indicates that the system behaves as a soft solid with limited viscous dissipation. Visual observations confirm these different behaviors.

The frequency dependence of the storage and loss moduli as a function of the polymer concentration in the regime $c > c^*$ can be observed for $\sigma = 0.5$ Pa in the insets of Figure 11. At 0.5 Pa, the system is the less affected by the shearing stress and the structure of the material is close to the initial and genuine one. For low polymer concentrations, the loss modulus G'' is larger than the storage modulus G' and the network behaves like a liquid. In this regime, the power law dependences of G' and G'' are described by exponents of approximately 1. It is difficult to say whether this contrasts the $G' \sim \omega^2$, $G'' \sim \omega$ Maxwellian relationship typically observed for telechelic polymers.[29,30] Many authors have identified the single Maxwell relaxation time observed in telechelic solutions with the exit rate of the hydrophobic part from the micellelike junction.[29] The viscoelastic properties of our system are different and are characterized by many long relaxation times that were recently described theoretically[28] (see section 3.4.2).

At this stage, it is important to observe the increase of G' and of the ratio G'/G'' on concentration. The evolution from a liquidlike behavior (Figure 11a) to a solidlike behavior (Figure 11c) clearly indicates a transition to a gel state. Also, at a high polymer concentration, G' and G'' are parallel as predicted for gels. Consequently, the number of mechanically active chains, that is, of bridges between hydrophobic cores, is clearly increasing with polymer concentration. The concentration-induced loop-to-bridge transitions and the interconnection by flower aggregates in the network are characteristic structural features of the system that are found to be consistent with viscosity and fluorescence results.

3.4.2. Zero-Shear Viscosity. The variation of the steady-state solution viscosity with shear rate for a 15×10^{-3}, 17×10^{-3}, 2×10^{-2}, and 10^{-1} g/cm^3 solution is given in Figure 4. Under increasing shear rate, a limited Newtonian plateau (shear-rate-independent viscosity) is followed by a shear-thickening regime at intermediate shear rates. After a given shear rate, a dramatic drop in the viscosity is observed. The shear-thinning behavior observed at elevated shear rates is even more pronounced for high polymer concentrations. The strong decrease of viscosity is usually observed in telechelic systems and is explained by the large change in the connectivity of the associative network, that is, bridge-to-loop transitions under shear.

A particular attention is drawn to the unusually high concentration dependence of the zero-shear viscosity η_0 in this regime $c \gg c^*$ (variation presented in Figure 2). Previous studies on HEUR (hydrophobically modified ethoxylated urethanes) telechelic polymers indicated a much lower variation and that the exponent describing the concentration dependence of η_0 was close[47] to 3.4: $\eta \sim c^{3.4}$. Recently, Semenov and Rubinstein[28] have developed a theory and have predicted an exponentially strong concentration dependence of η_0. They showed that the flower aggregates control both the equilibrium structure of the network and its dynamics. Flower micelles are hopping from one position to another, hence, diffusing. The micellar hopping time, τ_h, that corresponds to the terminal relaxation time of the system is exponentially longer than the chain conformation relaxation time (Rouse or reptation time if the chains are entangled) in the micellar gel; hence, relaxation of the micelle aggregates dominates the zero-shear-rate viscosity and $\eta_0 \sim G_m \tau_h$, where G_m is the elastic modulus corresponding to the deformation of micellar cells. This hopping process requires a high activation energy, which is in part due to the deformation of the aggregate and its neighbors (e.g., debridging mechanism). The relaxation time $\tau_{slow} \sim q^{-2}$ measured by DLS at low angles corresponds to the time of diffusion of free micellar aggregates and is much shorter than τ_h. We can obtain a characteristic structure relaxation time for the 10^{-1} g/cm^3 sample using the values of G_0 and η_0 deduced respectively from Figures 11 and 4 and the following equation:[48]

$$\eta_0 = \tau_R G_0 \tag{12}$$

where τ_R is the characteristic structure relaxation time and G_0 is the plateau modulus obtained at high frequency. Note that eq 12 is not necessarily valid for gels; however, we are only interested in the extraction of the order of magnitude of τ_R at 10^{-1} g/cm^3. For this concentration, we obtain a large value around 100 s for the characteristic time $\tau_R \sim \tau_h$. In particular, for high activation energy of sticker dissociation and when the number of monomers between entanglements is smaller than $m^{2/3}$, the dynamics is controlled by the collective tube leakage and[28]

$$\eta_0 \approx \exp(\text{const } c^{0.87}) \tag{13}$$

The fit of the high concentration regime presented in Figure 2 leads to $\eta_0 \sim \exp(\text{const } c^{0.52})$ and is in relative agreement with the already described theoretical considerations taking into account the limited number of data points and the poor accuracy of the viscosity estimations.

3.4.3. Shear-Thickening Behavior. The shear-thickening behavior has been observed in many telechelic systems[29,30] and in graft copolymer semidilute solutions, that is, hydrophobically modified polymers.[40,47,49] Also, several mechanisms have been proposed to explain this feature.[50−53] These mechanisms are usually based on models that describe the shear effects on the behavior of individual chains, that is, non-Gaussian chain deformation. Other models suggest a shear-induced increase of interpolymer associations yielding the formation of a temporary network. More recently, Tam et al.[29] have studied telechelic systems and have proposed a different interpretation using the superposition of dynamic oscillations on steady shear flow. They attributed the shear-thickening effect to the incorporation under shear of unassociated micelles or finite aggregates (microgels) that do not contribute to the plateau modulus into the percolation network of bridged flowerlike micelles coupled with the rearrangement of the superbridges to yield an increase in the number of junctions. This result suggested that the shear thickening is the result of a shear-induced increase in the density of mechanically active chains, which comes from an increase in the ratio of bridging to looping chains. Our experimental data are not sufficient to confirm this model. However, it is reasonable to consider that the behavior of our HMC is very similar to the one reported for these telechelic systems because the hydro-

(47) English, R. J.; Gulati, H. S.; Jenkins, R. D.; Khan, S. A. *J. Rheol.* **1997**, *41*, 427.
(48) Green, M. S.; Tobolsky, A. V. *J. Chem. Phys.* **1946**, *14*, 80.
(49) Aubry, T.; Moan, M. *J. Rheol.* **1994**, *38*, 1681.
(50) Savins, J. G. *Rheol. Acta* **1967**, *7*, 87.
(51) Vrahopoulou, V.; McHugh, A. J. *J. Non-Newtonian Fluid Mech.* **1987**, *25*, 157.
(52) Ballard, M. J.; Buscall, R.; Waite, F. A. *Polymer* **1988**, *29*, 1287.
(53) Witten, T. A.; Cohen, M. H. *Macromolecules* **1985**, *18*, 1915.

phobic degree of substitution of our alkyl chitosan is equal to 2%. This low degree of substitution allows easily the chain to form loops and then flowerlike aggregates. The distance between two hydrophobic grafts, ~250 Å, is likely comparable to the length of a bridge between two hydrophobic cores.

3.4.4. Shear-Thinning Behavior. The strong decrease of viscosity is indicative of the large change in the connectivity of the system under higher shear. Results presented in the previous parts allow us to confirm the idea of loop-to-bridge transitions in the buildup of the associative network with increasing polymer concentration in the regime $c \gg c^*$. In the shear-thinning regime, we observe bridge-to-loop transitions and then a structure breakdown under shear at elevated shear rates. In our case, by bridge-to-loop transitions, we mean an increase in the ratio of the number of looping chains to that of bridging chains. This behavior has already been proposed and described by Yekta et al.[54] for structures formed by telechelic polymers (HEUR) with end groups sufficiently hydrophobic to form flowerlike micelles. In their model, elevated shear rates cause the bridging chains to fragment, yielding smaller structures and discrete microgels. More recently, Tam et al.[29] ascribed the shear-thinning behavior in HEUR systems to a stress-induced decrease of the relaxation time of chain segments responsible for an increasing rate of rupture of bridges as the shear rate is increasing.

The behavior and the structure of semidilute solutions of telechelic systems and of associating polymers with many stickers per chain (with a low level of substitution) are somewhat similar; that is, we observe the formation of an associative network in which flower aggregates play the role of junctions.[28] If the stickers of associating polymers are sufficiently hydrophobic (like in our case), they will strongly associate to form large aggregates that control both the equilibrium structure of the system and its dynamics.[28] The association results in formation of micelles yielding a reversible gel phase of interconnected, closely packed micelles. In our study, the rheological behavior being similar to the one reported for HEUR systems, we attribute the large reduction in viscosity to bridge-to-loop transitions and then to microgels or a low-connected network formation under shear. Figure 7 describes the evolution of the associative structures of our system under dilution or shear. It is important to note that this flow-induced structure is reversible. Upon cessation of shear and after having performed a new experiment on the same sample, we have retrieved the equilibrium solution with the initial viscosity and elastic modulus.

3.5. Phase Separation $c_1 < c < c_2$. A phase separation between a solution and a solidlike gel (densely aggregated flower aggregates, that is, fully connected network) is observed for concentrations ranging from c_1 to c_2 (see Figure 1). In the case of hydrophobically end-capped linear polymers (or telechelic associating polymers), such as, for example, the so-called HEURs, a phase separation between a dilute solution of essentially separated flowerlike micelles and a dense phase of aggregated micelles is occasionally observed.[55−57] It is now well-known that the existence of a phase separation depends strongly on the length of the polymer backbone, the chemical nature of the hydrophobic terminal groups, and the degree of substitution as well as the length of the hydrophobic groups.[29,57−59] This phase separation has been predicted on the basis of theories of interacting polymer brushes. It originates from an entropic attraction of chain ends in neighboring micelles, which leads to bridging between micelles.[19] This theoretical prediction has been validated using experiments performed under hydrophobically modified polyoxyethylene chains.[56,57] For telechelic associating polymers, the concentrate phase consists of densely packed bridged flowerlike micelles, whereas the dilute phase can be seen as a gas of isolated flowers. Note that Le Meins and Tassin have reported a shear-induced phase separation.[30] The origin of the phase separation observed in our study for HMCs consisting of alkyl side chains grafted to the polyelectrolyte backbone is similar to the one reported for telechelic polymers (entropic origin). As a result of the low quantity of the two phases, it was difficult to study in detail the structure and the dynamics of these two characteristic separated phases. However, visual observations allow us to confirm that the behavior of the solidlike gel phase is similar to the one observed and studied at a high polymer content, that is, $c \gg c^*$ (cf. 10^{-1} g/cm^3). As for the phase in equilibrium with the gel one, we expect a micellar or a microgel solution.

4. Conclusion

In this study, we have examined the structural and dynamical properties of HMC associative networks. The strong hydrophobic character of the alkyl side chains and the low degree of substitution equal to 2% allow easily the chains to form loops and then flowerlike structures.

In the semidilute regime ($c > c^*$), SANS and DLS experiments (Figures 6, 8, and 9) have shown the presence of ~50-nm flower aggregates. In this regime, an open secondary association process leading to the formation of bridges between neighboring flower aggregates is occurring as the polymer concentration is increasing. A connected network is formed from the percolation of bridges leading to a large increase in solution viscosity (see Figure 2). In this regime, flower aggregates act as network junctions and are responsible for the $I(q) \sim q^{-3}$ SANS signal and for the slow mode measured in DLS.

Rheology measurements have shown that the increase in polymer concentration in the regime $c > c^*$ induces loop-to-bridge transitions. At a low polymer concentration, we observe a low-connected very weak network with formation of microgels under stress, whereas we obtain a rigid fully connected network and a solidlike rheological behavior at an elevated polymer content.

The variation of the steady-state viscosity with shear rate showed a behavior similar to the one reported for telechelic systems. Under increasing shear rate, we observed a Newtonian plateau followed by a shear-thickening regime at intermediate shear rates and a shear-thinning behavior at elevated shear rates. The strong decrease of viscosity is explained by the large change in the connectivity of the associative network, that is, bridge-to-loop transitions under shear. This study is the first one to our knowledge reporting combined SANS, light scattering, and rheology measurements performed on HMC solutions.

LA036395S

(54) Yekta, A.; Xu, B.; Duhamel, J.; Adiwidjaja, H.; Winnik, M. A. *Macromolecules* **1995**, *28*, 956.
(55) Kaczmarski, J. P.; Glass, J. E. *Macromolecules* **1993**, *26*, 5149.
(56) François, J.; Maître, S.; Rawiso, M.; Sarazin, D.; Beinert, G.; Isel, F. *Colloid Surf.* **1996**, *112*, 251.
(57) Pham, Q. T.; Russel, W. B.; Thibeault, J. C.; Lau, W. *Macromolecules* **1999**, *32*, 2996.
(58) Alami, E.; Almgren, M.; Brown, W.; François, J. *Macromolecules* **1996**, *29*, 2229.
(59) Ng, W. K.; Tam, K. C.; Jenkins, R. D. *J. Rheol.* **2000**, *44*, 137.